Review

Impact of Molecular Ligands in the Synthesis and Transformation between Metal Halide Perovskite Quantum Dots and Magic Sized Clusters

Li Liu, Keliang Pan,* Ke Xu, and Jin Z. Zhang*

Read Online

ACCESS | Metrics & More | Article Recommendations

ABSTRACT: Metal halide perovskite quantum dots (PQDs) and perovskite magic sized clusters (PMSCs) exhibit interesting size- and composition-dependent optoelectronic properties that are promising for emerging applications including photovoltaic solar cells and light-emitting diodes (LEDs). Much work has focused on developing new synthesis strategies to improve their structural stability and property tunability. In this paper, we review recent progress in the synthesis and characterization of PQDs and PMSCs, with a focus on the impact of different molecular ligands on their surface passivation and interconversion. Moreover, the effect of capping ligands on ion exchange during synthesis and doping is discussed. Finally, we present some perspectives on challenges and opportunities in fundamental studies and potential applications of both PQDs and PMSCs.
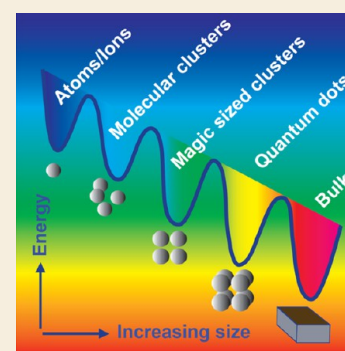
1. INTRODUCTION

Metal halide perovskites (MHPs) with an ABX_3 composition [A is an organic or inorganic cation, such as methylammonium ($CH_3NH_3^+$, MA^+), formamidinium ($CH(NH_2)_2^+$, FA^+), or cesium cation (Cs^+), B is a divalent metal ion such as Pb^{2+}, and X is halide ions][1] exhibit fascinating optoelectronic properties with promising applications in fields including photovoltaics (PVs),[2] light-emitting diodes (LEDs),[3] photodetectors,[4,5] and sensing.[6] Compared to bulk MHPs, perovskite quantum dots (PQDs) exhibit unique electronic and optical properties, including broadly tunable optical absorption and emission that depend on size, capping ligand, and composition desired for different applications,[7,8] similar to the behavior of the "benchmark" semiconductor quantum dots such as CdSe and CdS.[9] Also similar to chalcogenide clusters, perovskite magic sized clusters (PMSCs) have a single size or narrow size distribution and are smaller than PQDs.[10] Because magic sized clusters have higher monodispersity and smaller size compared to those of quantum dots, they could be used as a unique platform to study the growth mechanism of quantum dots.[11,12] Despite some similarities in electronic and optical properties, PQDs and PMSCs are structurally different from chalcogenide quantum dots and clusters. Clarifying the relation between PQDs and PMSCs can help to better understand the evolution of fundamental properties during transformation from individual ions to bulk MHPs, as present in Figure 1.

Due to the very large surface-to-volume (S/V) ratio and high reactivity of surface atoms, PQDs and PMSCs need to be protected for stability.[13] Passivation of surface dangling bonds or defect sites using molecular capping ligands with appropriate anchoring functional groups is a simple and effective strategy for surface protection and stability.[14] Interestingly, through ligand engineering and control of experimental conditions, PQDs can be transformed to PMSCs or vice versa.[15−17] In this review, we highlight the critical role of capping ligands in the surface passivation of PQDs and PMSCs with a number of examples. Furthermore, we present recent findings on the transformation between PQDs and PMSCs and related mechanisms. Additionally, the ligand effect on doping for doped PQDs and PMSCs is discussed. Finally, we present our perspectives for future studies of both PQDs and PMSCs.

2. ROLE OF CAPPING LIGANDS IN THE SYNTHESIS AND PROPERTIES OF PEROVSKITE QUANTUM DOTS AND PEROVSKITE MAGIC SIZED CLUSTERS
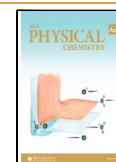
Generally, two wet chemical methods have been used for the preparation of PQDs: hot injection (HI)[18−22] and ligand-
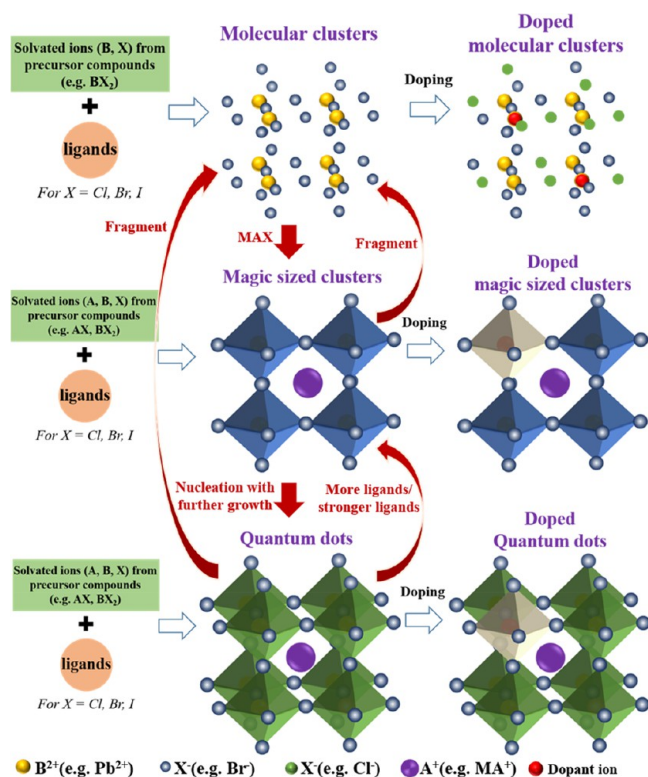
Figure 1. Schematic illustration of the synthesis of undoped and doped lead halide molecular clusters (MCs), PMSCs, and PQDs as well as their interconversion. For perovskites, MCs are synthesized only in the presence of PbX$_2$ (X for halide ions) and ligands, with no A component. With the addition of the A component precursor (e.g., MAX), MCs can be converted into PMSCs and further into PQDs. Conversely, with more ligands and/or stronger ligands, PQDs can be converted into PMSCs. PQDs and PMSCs can also fragment into MCs. The interconversion among MCs, PMSCs, and PQDs is strongly dependent on the experimental conditions, including the reactant concentration and ligand concentration. PQDs could be "precursors" to bulk perovskites under appropriate experimental conditions, such as removal of ligands.

assisted reprecipitation (LARP).[8,23] The HI approach relies on injection of a presynthesized precursor into an organic solvent containing another precursor ligands under high temperature (140−200 °C) and inert atmospheres, followed by quenching of the reaction with an ice bath. For example, HI was adopted to prepare CsPbX$_3$ PQDs by Protesescu et al. in 2015 for the first time.[24] This method generally produces well-defined colloidal PQDs, which enables control over size and stability via controlling reaction temperature and halide elements.[18−22] The LARP approach relies on the spontaneous crystallization of the material when it reaches a supersaturated state, which is carried out in the presence of capping ligands, and the nucleation and growth of the precipitate can be controlled. For instance, Zhang et al. employed the LARP approach to synthesize luminescent colloidal MAPbBr$_3$ PQDs for the first time.[25] In this synthesis, a mixture solution of precursor materials (MABr and PbBr$_2$) in good solvent, dimethylformamide (DMF) or dimethyl sulfoxide (DMSO), was injected into toluene or hexane to drive the precipitation of MAPbBr$_3$ PQDs. The LARP technique is simple and produces PQDs with high photoluminescence quantum yields (PLQYs) at room temperature.

However, PQDs have a high percentage of surface atoms or ions that are uncoordinated (dangling bonds) on the surface, resulting in a high density of surface defects and band gap states. The trap states in PQDs, like the trap states in CdSe and CdS quantum dots, can capture photoinduced electrons or holes, leading to nonradiative relaxation and quenching of PL, especially excitonic or band-edge PL.[26,27] Both experimental and theoretical studies have demonstrated that passivation of surface defects with ligands is important to the stability and functionality of PQDs. Appropriate capping ligands anchored to the surface defect sites of PQDs can not only passivate surface defects and reduce associated trap states but also protect them from interacting and reacting with environment species such as water (H$_2$O) and oxygen (O$_2$).

For PQDs, there are at least three types of surface defect sites, which are associated with the three constituting components: inorganic/organic cation (A$^+$), divalent metal cation (B^{2+}), and halide anion (X$^-$). Combinations of organic carboxylic acids, such as oleic acid (OA), and amines, such as oleylamine (OLA), have been found to be highly effective for PQD passivation.[28] This can be attributed to protonation transfer between the carboxylic acid (−COOH) and amino (−NH$_2$) groups that results in negatively charged carboxylate (−COO$^-$) and positively charged ammonium (−NH$_3^+$) groups that are effective in passivating cationic (A$^+$ or B^{2+}) and anionic (X$^-$) surface defect sites, respectively.[29] The binary ligand strategy generally produces well-defined PQDs with narrow size distribution and good stability. Other straight chain capping ligands used include *n*-octanoic acid (OcA)/ valeric acid (VA) and *n*-octylamine (OcAm)/butylamine (BTYA).[17] A structural model of PQD passivated by linear carboxylic acid and amine capping ligands is shown in Figure 2a.[29]

The detailed structure of capping ligands has been found to play an important role in the effectiveness of surface passivation owing to their different strengths of binding to defects and steric hindrance effects. For instance, (3-aminopropyl)triethoxysilane (APTES) and polyhedral oligomeric silsesquioxane (POSS) PSS-[3-(2-aminoethyl)amino]-propylheptaisobutyl-substituted (NH$_2$-POSS) with short branched chains have been used as capping ligands to generate MAPbBr$_3$ PQDs.[30] Unlike PQDs capped with linear ligands, NH$_2$-POSS- and APTES-capped PQDs show higher stability as a result of the strong steric hindrance because of their cage-like or cone-shaped structure, respectively. Importantly, APTES-capped PQDs show improved stability in protic solvents, such as isopropyl alcohol, compared to that of NH$_2$-POSS-capped PQDs. This is attributed to a thin layer of silica generated on the PQDs' surface due to hydrolysis of APTES. The silica layer can further prevent H$_2$O, O$_2$, and other protic solvent molecules from reaching and reacting with the PQD core, as illustrated in Figure 2b. The improved stability of PQDs using branched capping ligands is important for device applications.

Likewise, Vickers et al. introduced conductive aromatic capping ligands, that is, benzylamine (BZA) and benzoic acid (BA), in the synthesis of MAPbBr$_3$ PQDs.[31] Due to the π−π stacking interaction between benzene rings of ligands, the PQDs exhibit higher conductivity and more efficient charge extraction compared to those of PQDs with long alkyl chains and alkoxysilane ligands (Figure 2c). Subsequently, the same approach has been demonstrated by using *trans*-cinnamic acid (TCA) and its derivates in combination with 3,3-diphenylpropylamine (DPPA) to passivate MAPbBr$_3$ PQDs.[32] TCA and its
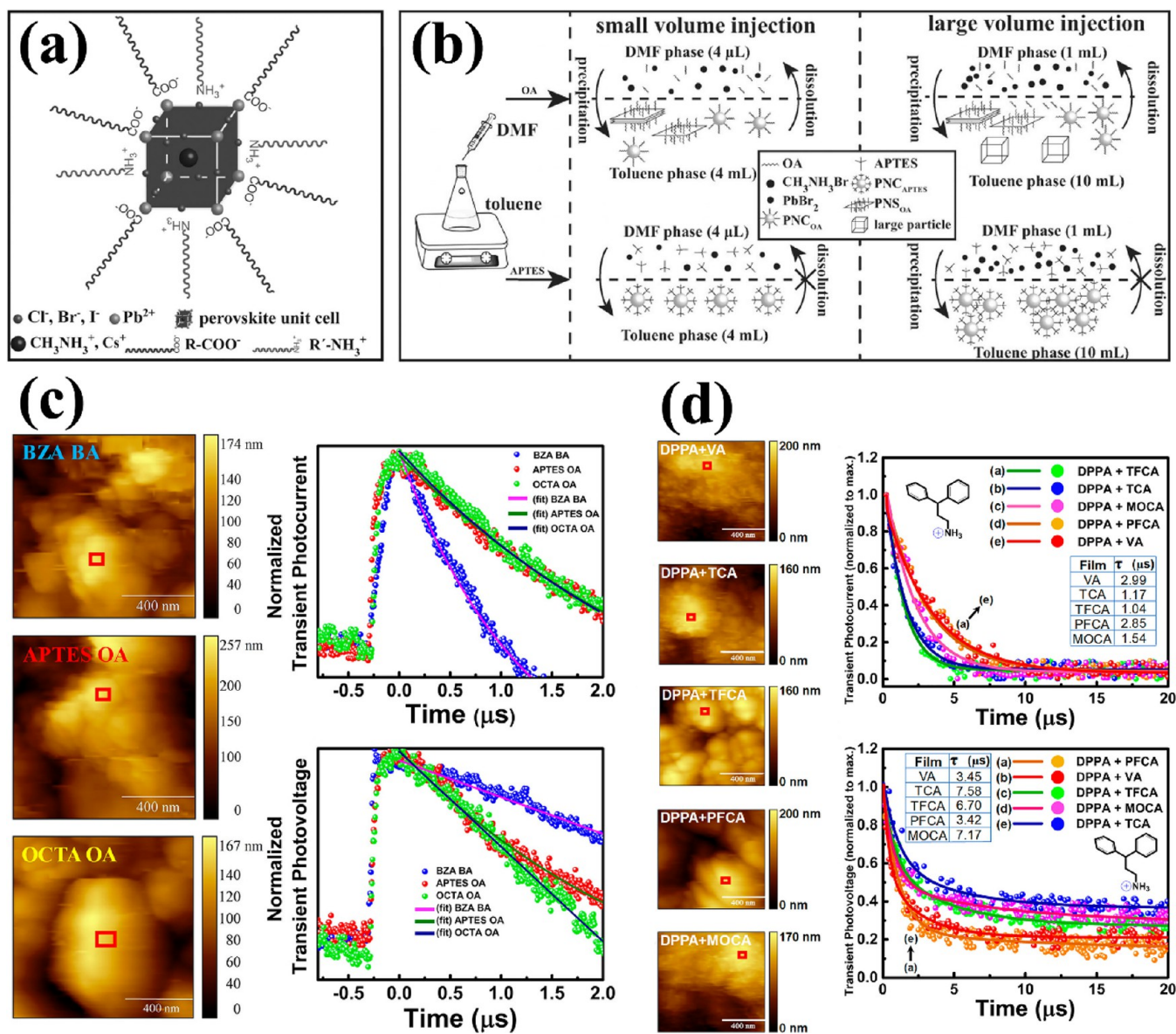
Figure 2. (a) Structural model of PQDs passivated by linear carboxylic acid and amine capping ligands. Reproduced with permission from ref 29. Copyright 2017 Wiley. (b) Influence of OA and (3-aminopropyl)triethoxysilane (APTES) ligand capping effects on the synthesis of MAPbBr$_3$ PQDs. Reproduced with permission from ref 30. Copyright 2016 Wiley. (c) Left image, from top to bottom, is the atomic force microscopy (AFM) topography images of MAPbBr$_3$ PQDs films with benzylamine (BZA)/benzoic acid (BA), APTES/OA, octylamine (OCTA)/OA capping ligands, and the right image, from top to bottom, is the normalized transient photocurrent (TPC) and transient photovoltage (TPV) decay curves from the corresponding PQDs. Reproduced from ref 31. Copyright 2018 American Chemical Society. (d) Left image, from top to bottom, is AFM topography images of 3,3-diphenylpropylamine (DPPA)/VA, DPPA/*trans*-cinnamic acid (TCA), DPPA/*trans*-4-(trifluoromethyl) cinnamic acid (TFCA), DPPA/*trans*-2,3,4,5,6-pentafluorocinnamic acid (PFCA), DPPA/*trans*-4-methoxycinnamic acid (MOCA) MAPbBr$_3$ PQDs films, and the right image, from top to bottom, is TPC and TPV decay curves from the corresponding PQDs. Reproduced from ref 32. Copyright 2020 American Chemical Society.

derivatives [i.e., *trans*-4-(trifluoromethyl)cinnamic acid (TFCA), *trans*-2,3,4,5,6-pentafluorocinnamic acid (PFCA), and *trans*-4-methoxycinnamic acid (MOCA)] are used as passivating exciton delocalized ligands (EDL) to reduce the energy gap relative to the PQD core, and the DPPA ligand stabilizes the PQD surface through π−π stacking intermolecular interactions and slows down charge trapping and nonradiative decay (Figure 2d).

In addition, multidentate ligand molecules, such as bidentate peptide-like ligands,[29] proteinogenic essential amino acids,[33−37] and zwitterionic surfactants,[38,39] that can provide multiple functional groups in one molecule have also been

used as capping ligands in the synthesis of PQDs. For example, Luo et al. used 12-aminododecanoic acid (12-AA), 8-aminooctanoic acid (8-AA), or 6-aminohexanoic acid (6-AA) as capping ligands in the synthesis of MAPbBr$_3$ PQDs.[29] The size and optical properties of PQDs can be tuned by adjusting the concentration of the peptide-like molecules as ligands (Figure 3a). A single peptide containing both −NH$_2$ and −COOH groups can effectively passivate PQDs, which is simpler than using two separate molecule ligands. The advantage of using peptide-like molecules as ligands is the presence of amphiphilic bifunctional groups in a single molecular. Such PQDs containing peptides on their surface
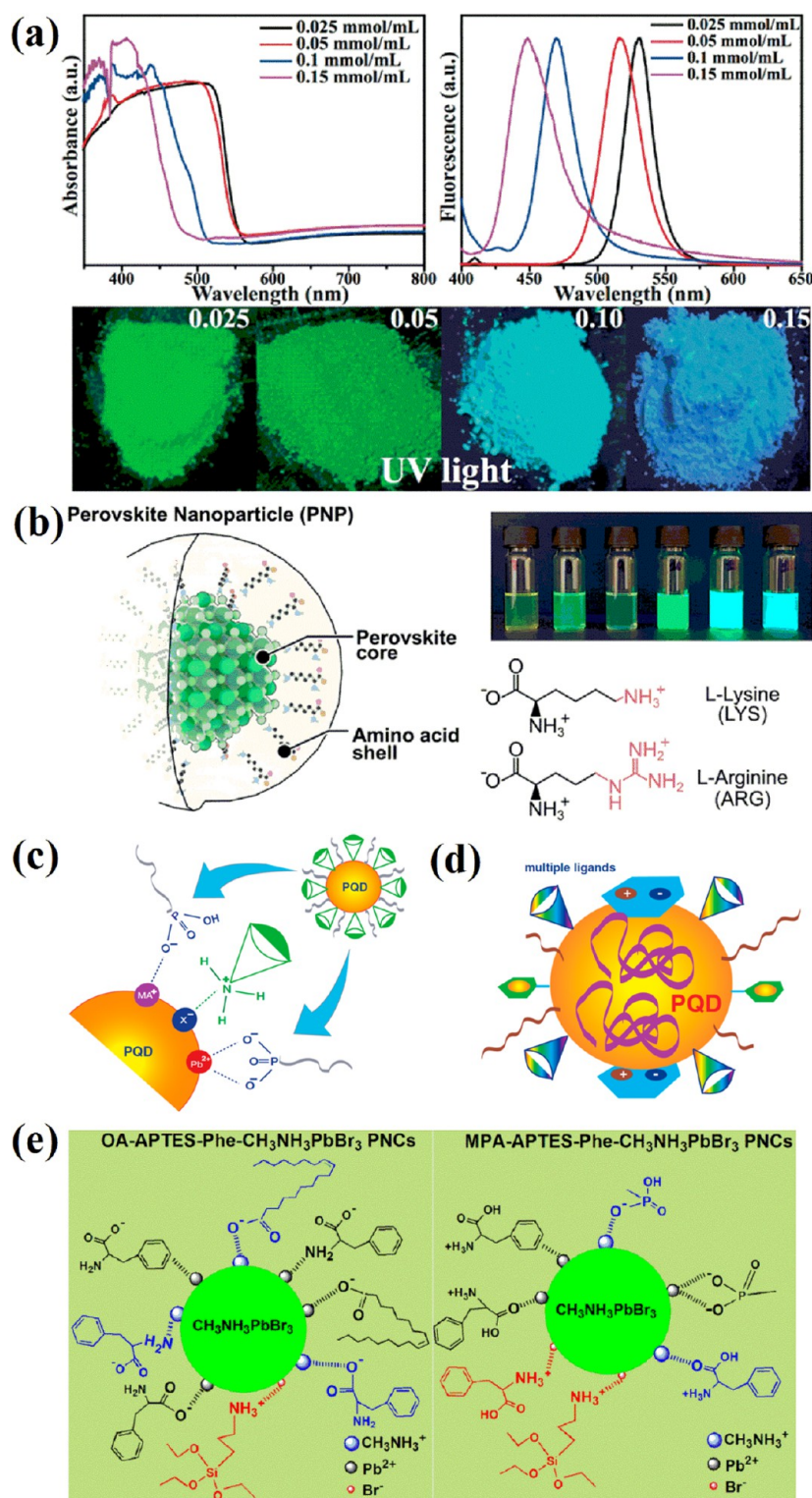
Figure 3. Surface passivation strategies of PQDs. (a) UV−vis absorption, PL spectra (λ_{ex} = 365 nm), and UV light (λ_{ex} = 365 nm) photographs of MAPbBr$_3$ PQDs prepared with 0.025, 0.05, 0.1, and 0.15 mmol·L^{-1} 12 AA. Reproduced with permission from ref 29. Copyright 2017 Wiley. (b) Schematic illustration of synthesis of MAPbBr$_3$ PQDs capped with L-lysine (Lys) and L-arginine (Arg) ligands. Reproduced from ref 33. Copyright 2019 American Chemical Society. (c) Schematic illustration of the passivation mechanism of MAPbBr$_3$ PQDs with phosphonic acids (PAs) and APTES ligands. Reproduced with permission from ref 40. Copyright 2019 Wiley. (d) Structural model for surface passivation of PQDs with multiple defects using a combination of ligands in a cocktail approach. Reproduced from ref 28. Copyright 2019 American Chemical Society. (e) Ligand binding models on the surface of MAPbBr$_3$ PQDs capped with phenylalanine ligands. Reproduced from ref 37. Copyright 2021 American Chemical Society.

have potential applications in the biomedical fields, including optical sensing and imaging. Similarly, Sharma et al. reported

the synthesis of MAPbBr$_3$ PQDs with excellent optical properties using amino acids [i.e., phenylalanine (Phe) and
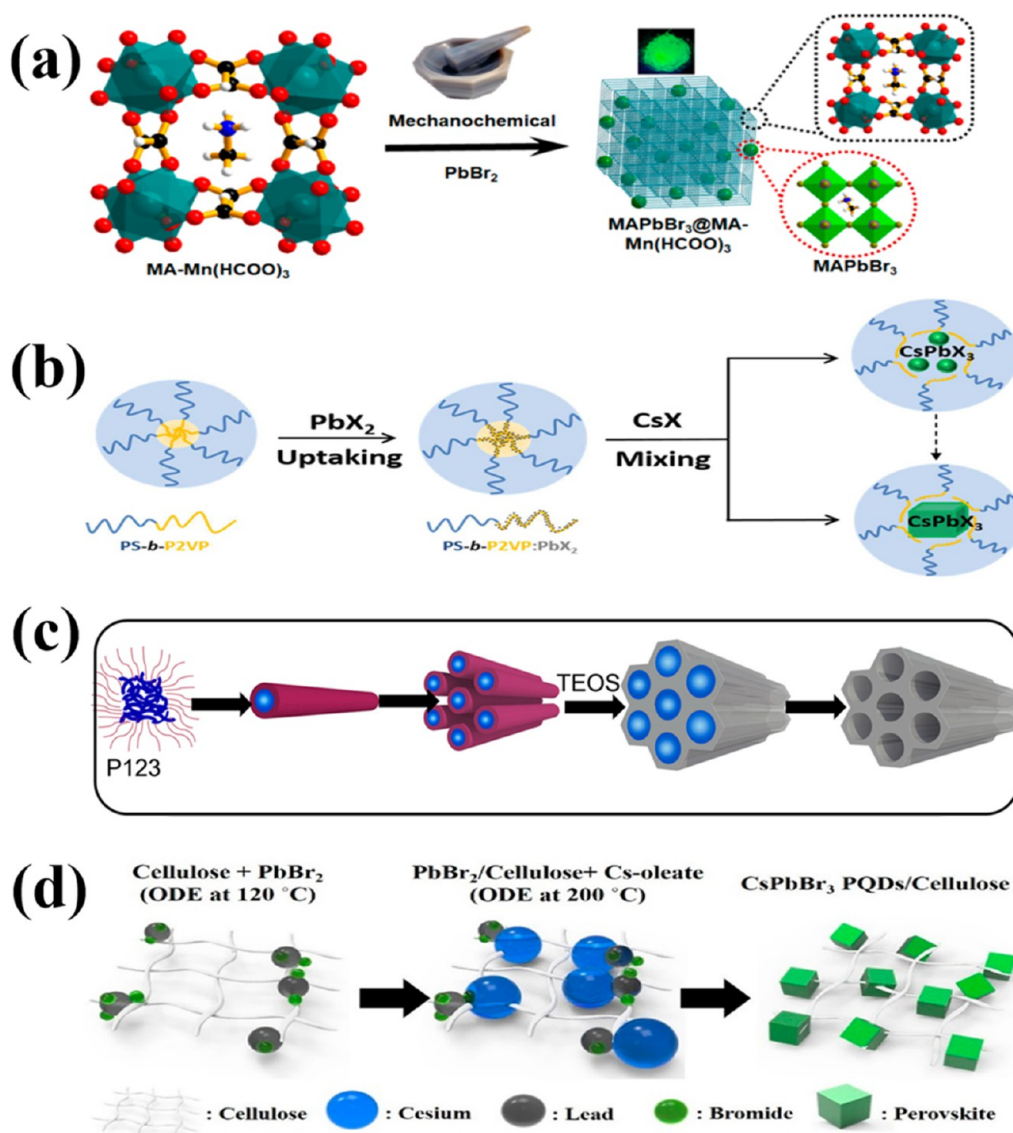
Figure 4. (a) Model for synthesis of MAPbBr$_3$ PQDs on metal−organic frameworks (MOFs). Reproduced from ref 45. Copyright 2020 American Chemical Society. (b) Synthesis of MAPbBr$_3$ PQDs using amphiphilic block copolymer micelles. Reproduced from ref 46. Copyright 2017 American Chemical Society. (c) Synthesis of molecularly imprinted mesoporous silica embedded with CsPbBr$_3$ PQDs. Reproduced with permission from ref 47. Copyright 2020 Elevier. (d) Synthesis of CsPbBr$_3$ PQDs/cellulose composite. Reproduced from ref 48. Copyright 2020 American Chemical Society.

leucine (Leu)] as ligands.[34] During nucleation, the carboxylic group coordinates with the B^{2+} ions, while the amino group terminates the growth and stabilizes the PQDs. Likewise, Jancik Prochazkova et al. reported the use of L-lysine (Lys) and L-arginine (Arg) for PQD surface passivation.[33] The visible light emission bandwidth of the obtained MAPbBr$_3$ PQDs is narrow, with PLQYs close to 100%. In addition, preferential ligand orientation was achieved via the α-amino group blocking, with *tert*-butyloxycarbonyl (*t*Boc), which resulted in blue-shifted emission with smaller and more uniform particles, as shown in Figure 3b. These results demonstrate the effectiveness of peptide-like or natural proteinogenic amino acids as surface ligands to stabilize and modify PQDs.

The acid−base proton exchange strategy was later expanded to phosphonic acids (PAs) and amine as an acid−base pair of capping ligands. Xu et al. reported the first combination of PAs with APTES as a dual passivation system during the synthesis of MAPbBr$_3$ PQDs.[40] PAs can protonate −NH$_2$ to −NH$_3^+$ and

generate −PO$_3^{2-}$ and −PO$_2$(OH)$^-$ anions. The Pb^{2+} and MA$^+$ surface defects can be passivated by −PO$_3^{2-}$ or −PO$_2$(OH)$^-$, whereas Br$^-$ surface defects are likely passivated by −NH$_3^+$. Additionally, the −PO$_3^{2-}$ has a more stable tripod resonance structure than −COO$^-$, which may better passivate the surface, as shown in Figure 3c.

Based on a number of studies involving the use of ligand combinations, a "cocktail" approach was proposed as a general strategy for effective passivation of PQDs, as illustrated in Figure 3d.[28] Following this strategy, Liu et al. combined Phe with APTES and OA or methylphosphoric acid (MPA) as capping ligands to improve the PL and stability of MAPbBr$_3$ PQDs.[37] Phe can passivate the surface defects by coordinating with A$^+$ or B^{2+} ions using its lone pair electrons on the N atom in the −NH$_2$ group or O in the −COOH group. The form in which Phe exists also depends on the pH of the solution. When the pH is greater than the isoelectric point of Phe, Phe is in its anionic state (H$_2$N−C$_8$H$_8$−COO$^-$) and is expected to bind to
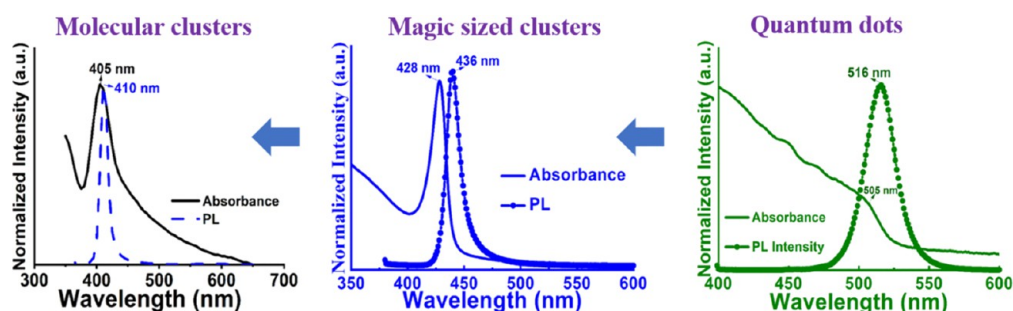
Figure 5. UV−vis absorption and PL spectra of MCs, PMSCs, and PQDs. For PQDs, the excitonic absorption peak is around 505 nm, and the PL emission peak is around 516 nm. For PMSCs, the excitonic absorption peak is around 428 nm, and the PL emission peak is around 436 nm. For MCs, the excitonic absorption peak is around 405 nm, and the PL emission peak is around 410 nm.

A^+ or B^{2+} defect sites through electrostatic interaction. When the pH is lower than the isoelectric point of Phe, Phe is positively charged ($^+H_3N-C_8H_8-COOH$) and can passivate X^- defect sites, as illustrated in Figure 3e.

Recently, alkylammonium ions have been studied as capping agents in the synthesis of $CsPbBr_3$ PQDs to improve their phase stability, control size, and enhance PLQYs.[41−43] Classical molecular dynamics simulations have been carried out to gain insights into the intrinsic binding properties of primary dodecylammonium (DA), secondary didodecylammonium (DDA), and quaternary dimethyldidodecylammonium (DMDDA).[42] It was found that DDA was loosely bound to the surface of $CsPbBr_3$, whereas the coverage of DMDDA was more stable than that of the primary oleylammonium ligand. Enhanced binding strength was attributed to the ability of the ligand headgroup to penetrate the binding pocket and weak interaction of the headgroup with polar acetone solvent molecules.

Pradhan reviewed the interactions of alkylammonium ions on the surface of perovskite nanocrystals and their effect on surface reconstruction.[43] During the nucleation and growth of $CsPbX_3$ nanocrystals, there is a competition between alkylammonium and Cs^+. Under different conditions, the treatment of excess alkylammonium ions can lead to the formation of multifaceted polyhedron nanocrystals. New surface ligands with special binding capabilities are required to stabilize the new facets and thereby adjust their shapes.[44]

Despite the success of ligand passivation in the synthesis of high-quality PQDs, surface ligands often tend to be labile in solution. To address this issue, polymers or inorganic matrices have been employed to passivate PQDs and to improve stability against O_2, light, and heat (Figure 4). For instance, Rambabu et al. reported the mechanochemical stabilization of $MAPbBr_3$ PQDs within perovskite metal−organic frameworks (MOFs) $[MA-M(HCOO)_3]$ (M = Mn and Co) (Figure 4a).[45] The perovskite MOFs serve as a template and source for MA^+ in growing and stabilizing PQDs. The resulting $MAPbBr_3@MA-Mn(HCOO)_3$ composites exhibit excellent chemical stability and good photoelectrochemical activity, which can be used for H_2O splitting or CO_2 reduction. Similarly, Hou et al. employed polystyrene-*block*-poly-2-vinylpyridine (PS-*b*-P2VP) as a micelle template to create PQDs with a multidentate polymer nanoshell (Figure 4b).[46] The stability of these PQDs in both colloidal and thin film forms is orders of magnitude improved. The copolymer acts as a confined nanoreactor during perovskite crystallization and passivates the surface by forming a multidentate capping layer, thereby improving photostability in polar solvents. Similarly, Huang et

al. reported the preparation of PQDs with uniform size and high PLQYs using molecularly imprinted mesoporous silica (Figure 4c).[47] Mesoporous silica can encapsulate functional nanoparticles based on their well-ordered channels, large pore volume and specific surface area, and easy modification. Likewise, Park et al. synthesized a $CsPbBr_3$ PQDs/cellulose composite (Figure 4d),[48] in which the strong adhesion between PQDs and porous cellulose fibers helped to improve stability and durability under various humidity conditions, as well as superior PL property. Imran et al. reported synthesis of $APbX_3$ PQDs encapsulated in poly(acrylic acid)-*block*-poly-(styrene) (PAA-*b*-PS) micelles.[49] Nuclear magnetic resonance (NMR) analysis shows that the polymeric micelles embedded with PQDs have a core−shell structure, with PAA forming the core of the micelle and PS the outer layer. On one hand, the polymer serves as a protective layer to isolate the PQDs from the surrounding environment, making them less reactive. On the other hand, the polymer is extended in solution, exposing part of the surface of PQDs to the surrounding media, resulting in a series of chemical reactions with the PQDs and making them "reactive".

Compared to PQDs, PMSCs are smaller nanoparticles with single size or highly uniform size distribution. Due to the ultrasmall size and tendency to grow into larger particles such as PQDs upon drying, PMSCs cannot be measured easily by transmission electron microscopy (TEM) or X-ray diffraction (XRD). Their low stability at elevated temperature makes it generally hard to study using mass spectrometry. Instead, the main evidence for PMSCs is from spectroscopy, with sharp, well-defined, and significantly blue-shifted absorption and emission bands compared to those in the bulk and PQDs (Figure 5).[15−17]

For PMSCs, the passivation strategy is very similar to that for PQDs. The main difference is that PMSCs have a larger S/V ratio and thus require better protection by ligands.[50] For example, Xu et al. reported the LARP synthesis of $CsPbBr_3$ PMSCs using OA and OLA as ligands.[51] Compared with the synthesis of $CsPbBr_3$ PQDs, the amount of OA/OLA ligands is much higher.

Inorganic capping ligands have also been used in the synthesis of PMSCs. Xu et al. found that trivalent metal-hydrated nitrate coordination complexes can act as ligands to control the LARP synthesis of $CsPbBr_3$ PMSCs.[52] With increasing aluminum nitrate nonahydrate $[Al(NO_3)_3·9H_2O,$ ANN] concentration, the solution changes from green to blue under UV light; the average PL lifetime (τ_{ave}) decreased from 7.29 to 1.36 ns, and the stability in water was improved, as shown in Figure 6. Also, the UV−vis and PL spectra show
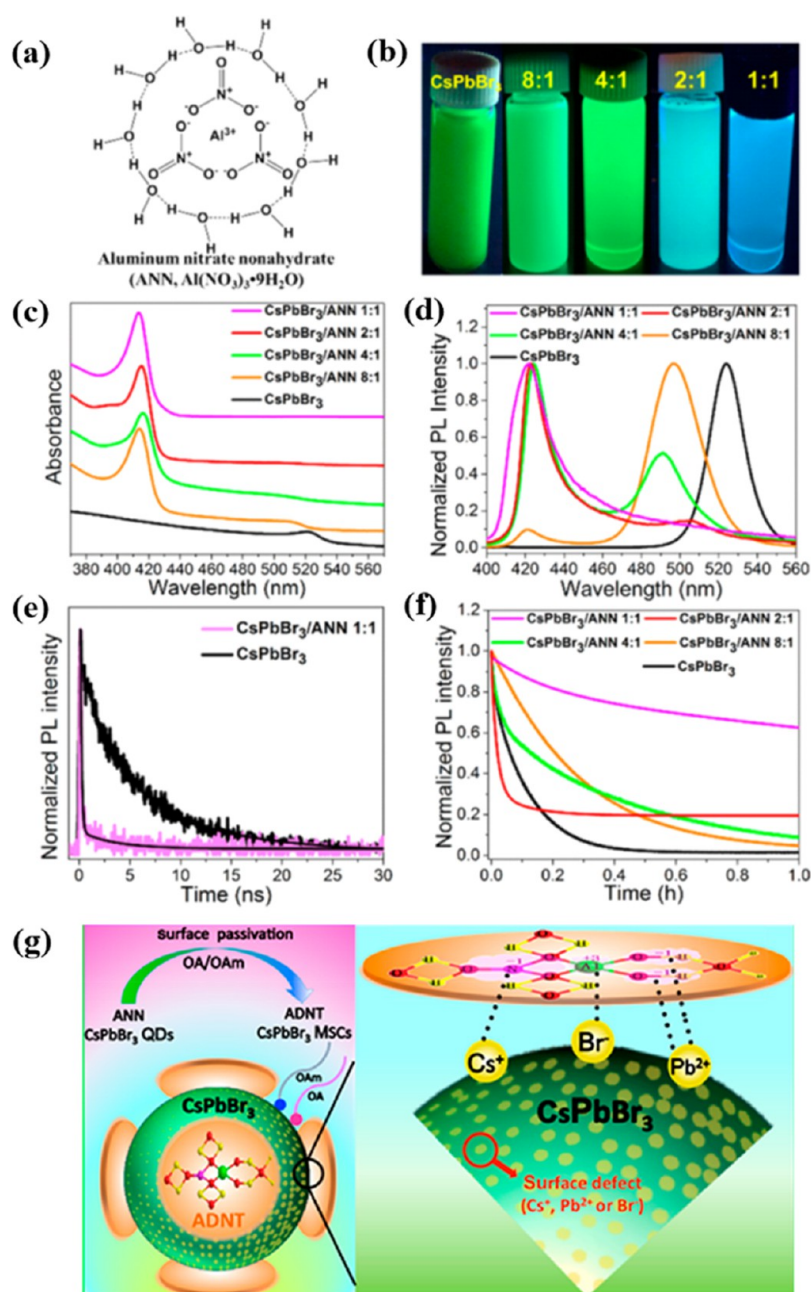
Figure 6. (a) Structure of aluminum nitrate nonahydrate ($Al(NO_3)_3 \cdot 9H_2O$, ANN). (b) Photograph of the samples under UV lamp irradiation (λ_{ex} = 365 nm). (c) UV–vis absorption vertically offset from each other. (d) PL spectra for the $CsPbBr_3$, and $CsPbBr_3$/ANN samples with molar ratios of 8:1, 4:1, 2:1, and 1:1. (e) Normalized time-resolved PL (TRPL) decay curves of the $CsPbBr_3$ sample and the $CsPbBr_3$/ANN sample with a molar ratio of 1:1. (f) Stabilities of the samples determined using a water test, where the relative fluorescence intensity of the precipitate was a function of water exposure time. (g) Surface passivation mechanism of $CsPbBr_3$ PMSCs with OA/OAm/ANN capping ligands. Reproduced from ref 52. Copyright 2019 American Chemical Society.

significant changes with the excitonic peak at ~520 nm, due to PQDs, changing to ~420 nm, which is attributed to PMSCs. It was proposed that, with the assistance of OA and OLA, ANN was transformed into aluminum dihydroxide nitrate tetrahydrate ($[Al(OH)_2(NO_3)] \cdot 4H_2O$, ADNT). ADNT serves as a strong ligand with its NO_3^- and OH^- groups bound to Cs^+ and Pb^{2+} defect sites and Al^{3+} bound to Br^- defect sites. Compared to ligands with linear and umbrella structures, this planar binding configuration provides better protection and prevents molecules such as H_2O or O_2 from reaching the perovskite surface to cause degradation.

3. TRANSFORMATION BETWEEN PEROVSKITE QUANTUM DOTS AND PEROVSKITE MAGIC SIZED CLUSTERS

Capping ligands have been used to not only stabilize PQDs and PMSCs but also control the transformation between them.[53,54] For example, $CsPbBr_3$ PQDs can be transformed into PMSCs by increasing the concentration of organic carboxylic acids, mesitylacetic acid (MAA), OA, and phenylacetic acid (PAA), along with BZA as capping ligands (Figure 7a).[15] The concentration of organic carboxylic acid affects the exciton absorption of both $CsPbBr_3$ PMSCs and PQDs, with
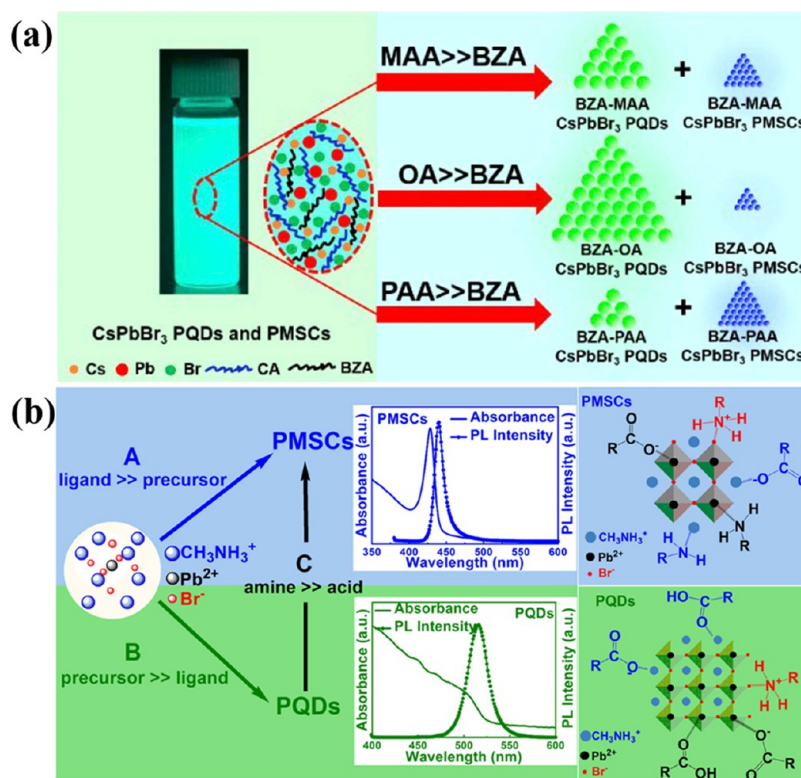
Figure 7. (a) Schematic illustration of the growth mechanism of CsPbBr$_3$ PQDs and PMSCs at room temperature and their dependence of transformation on the amount and type of organic carboxylic acids. Reproduced with permission from ref 15. Copyright 2020 Elsevier. (b) Schematic illustration of the growth mechanism of MAPbBr$_3$ PQDs and PMSCs and dependence of their conversion on the amount and ratio of ligands. Reproduced from ref 17. Copyright 2020 American Chemical Society.

higher concentration favoring PMSCs. A high concentration of PAA could generate pure CsPbBr$_3$ PMSCs, but the same concentration of MAA or OA could not, indicating that PAA is a stronger ligand. In addition, the ratio between organic carboxylic acid to BZA is also a key factor affecting the passivation effect.

Similarly, Liu et al. found that by changing the concentration of ligands (OcA/OA and OcAm/BTYA), the perovskites can be tuned between MAPbBr$_3$ PQDs and PMSCs (Figure 7b).[17] When the precursor/ligand ratio is high and there is excess organic acid ligand, PQDs can be obtained. The proton transfer reaction between the acid and amine ligand results in −COO$^-$ binding to MA$^+$ or Pb^{2+} and −NH$_3^+$ binding to Br$^-$. Excess organic acid ligand can also passivate the cationic defect sites by the lone pair of electrons in the O atoms in the −COOH group. When the ligand/precursor ratio is high and there are excess amine ligands, PMSCs can be obtained. The lone pair electrons on the N atoms of the amine ligands can interact with Pb^{2+} or MA$^+$. Meanwhile, a high concentration of the ligands helps to push the protonation reaction to generate more −NH$_3^+$ and −COO$^-$ that can more effectively passivate the surface defects. These studies show that stronger binding ligands or higher concentrations of ligands favor PMSCs over PQDs.

In a related study, in attempt to understand the growth mechanism of PMSCs, Vickers et al. found a new absorption peak at 402 nm and a new PL peak at 410 nm appeared, which are blue-shifted by about 20 nm compared that of PMSCs (Figure 8a).[10,16] Since this new species can be formed from PMSCs or synthesized directly with only PbBr$_2$ and BTYA present in the precursor solution without the A component, it

does not have the full perovskite structure. Therefore, this species was attributed to molecular clusters (MCs).[10] X-ray absorption spectroscopy and Fourier transformed extended X-ray absorption fine structure (FT-EXAFS) spectroscopy were used to elucidate the structure of MCs and suggest that BTYA coordinates with Pb^{2+} through the lone pair electrons of the amine functional group. Interestingly, by adding MABr, MCs can be converted into PMSCs. Therefore, MCs and PMSCs can be interconverted by varying the experimental conditions.

Another interesting finding is that PMSCs can be simply tuned by diluting the synthesized solution in toluene. By controlling the dilution and concentration of the ligand, the PL peak was blue-shifted from 438 to 410 nm (Figure 8b). This process is similar to the process of synthesizing perovskite nanoplatelets with a controlled size, in which the thickness of the nanoplatelets can be controlled both by degree of dilution and by ligand concentration.[55] The PMSCs may have fragmented into smaller discrete species. One can also start from precursor ions to form MSCs first and then convert them into MCs.[10]

4. DOPING OF PEROVSKITE QUANTUM DOTS, PEROVSKITE MAGIC SIZED CLUSTERS, AND LEAD HALIDE MOLECULAR CLUSTERS

Doping is a common and powerful approach to altering electronic, optical, and magnetic properties of semiconductors by replacing a small amount of one or more of the host ions with another ion or dopant.[56] Doping at different host lattice sites has different effects on the crystal structure and electronic band structure of the host. For example, a small amount of different dopants can be added into the A site to change the
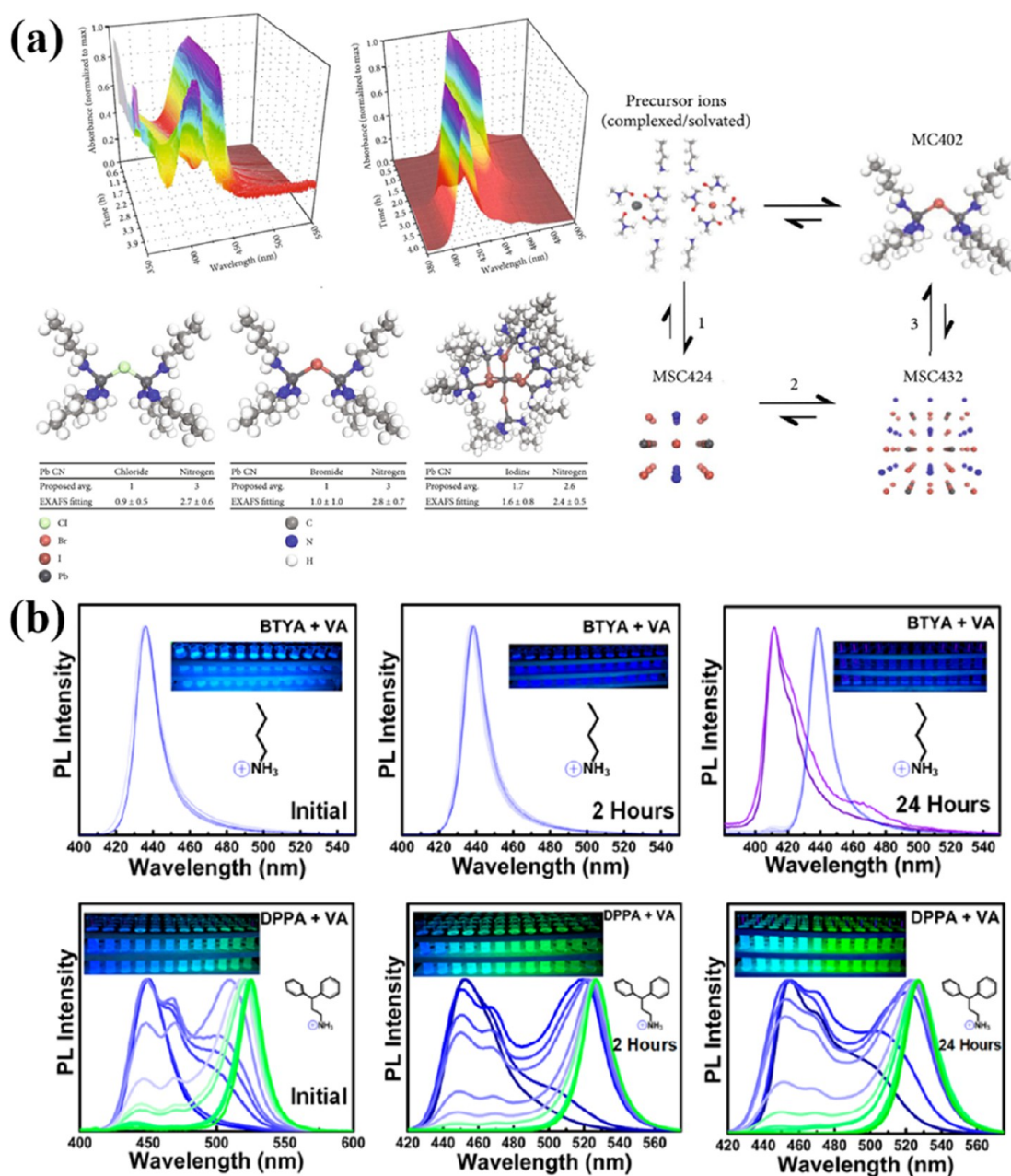
Figure 8. (a) Image on the left is the absorption and PL spectra overtime of MAPbBr$_3$ PMSCs. The lower left image is the molecular models and the Pb CN from the proposed model and EXAFS fitting results for MCs. The image on the right is the scheme illustrating the relation among precursor ions, MCs, and PMSCs. Reproduced with permission from ref 10. Copyright 2021 American Association for the Advancement of Science. (b) PL spectra of PMSCs in a series dilution. PL spectra were measured during the initial dilution and then after 2 and 24 h. The insets contain digital photographs after each measurement. Reproduced from ref 16. Copyright 2019 American Chemical Society.

tolerance factor and electronic properties of the perovskites, while the doping substitution of the B site can reduce the Pb^{2+} toxicity, and the X site doping can regulate the band gap of the perovskites. The introduction of dopant elements at specific locations provides an effective solution for improving the stability of the perovskite crystal structure, optimizing luminescence performance, improving nonradiative recombination, and regulating exciton dynamics (Figure 9a).[57−63] Among them, doping different cations at the B site can improve the phase stability, enhance the PL emission intensity, and reduce the toxic Pb content.[64]

While pristine perovskites usually have high PLQY and a small Stokes PL shift, it is sometimes desired for the large

Stokes shift to reduce self-absorption of the samples. In addition, it is useful to be able to further tune the PL emission for certain applications. One way to achieve the above is to dope the perovskites with emissive dopants. For example, doping with Mn^{2+} has been demonstrated for PMSCs, MCs, as well as PQDs, where optical reabsorption is reduced by decoupling the Mn^{2+} emission from the absorption of the perovskite host, due to the large Stokes shift of the dopant emission.[65] Xu et al. reported the first synthesis of Mn-doped CsPbBr$_3$ PMSCs with BA and BZA as passivation ligands and MnCl$_2\cdot$4H$_2$O and MnBr$_2$ as Mn^{2+} doping sources.[66] An equal molar ratio of BA/BZA as capping ligands results in the formation of CsPbBr$_3$ PQDs, whereas CsPbBr$_3$ PMSCs start to
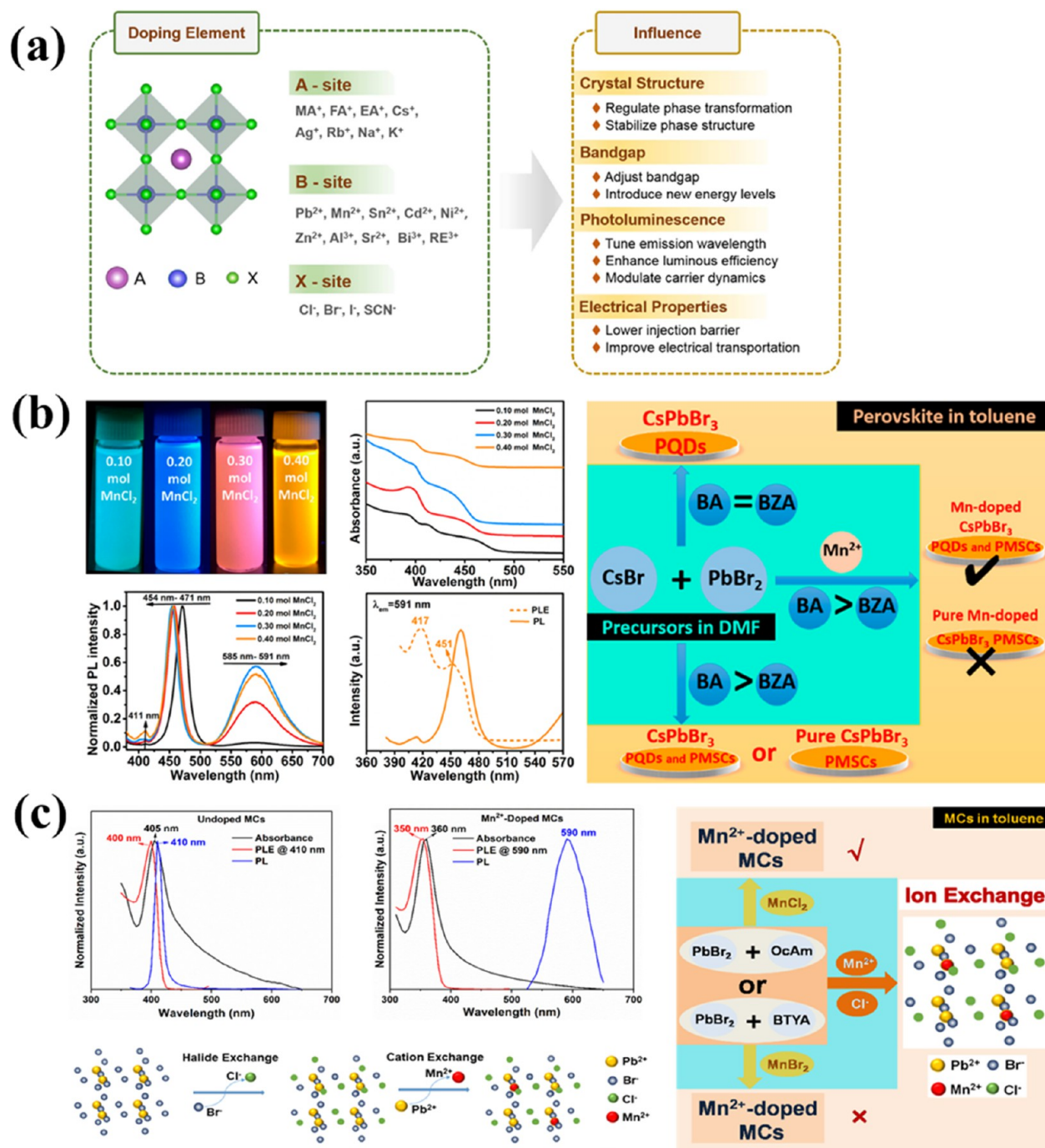
Figure 9. (a) Schematic diagram of the doped ions in ABX$_3$ perovskites and their corresponding influences on the material properties. Reproduced with permission from ref 57. Copyright 2019 Elsevier. (b) Photograph of the samples in toluene under UV lamp irradiation (λ_{ex} = 365 nm); UV−vis absorption and PL spectra for Mn-doped CsPbBr$_3$ PQD and PMSC samples with 0.10, 0.20, 0.30, and 0.40 mol MnCl$_2$·4H$_2$O; PL and PLE spectra of Mn-doped CsPbBr$_3$ PQD and PMSC samples with 0.40 mol MnCl$_2$·4H$_2$O; and schematic representation of Mn-doped and undoped CsPbBr$_3$ PMSC and PQD preparation. Reproduced from ref 66. Copyright 2020 American Chemical Society. (c) Optical properties of undoped and Mn-doped MCs. UV−vis absorption (black), PL (blue), and PLE (red) spectra of undoped and Mn-doped MCs, and schematic illustration of Mn-doped amino lead halide MCs. Reproduced from ref 67. Copyright 2021 American Chemical Society.

be produced when the molar ratio of BA/BZA is larger than 1. Interestingly, for Mn-doped samples, even with a larger BA/BZA ratio that produced pure undoped CsPbBr$_3$ PMSCs, only a mixture of Mn-doped CsPbBr$_3$ PMSCs and PQDs can be produced (Figure 9b). The concentration of Mn^{2+} affects the optical properties of PMSCs and PQDs, with a higher concentration of Mn^{2+} favoring CsPbBr$_3$ PMSCs over PQDs and resulting in a bluer absorption. The salt of Mn^{2+} also

influences the final doped products. Mn^{2+} changed the original acid/base equilibrium in the solution and facilitated the growth of CsPbBr$_3$ PMSCs into larger CsPbBr$_3$ PMSCs or CsPbBr$_3$ PQDs. Compared with MnBr$_2$, Mn^{2+} doping is more easily achieved with MnCl$_2$·4H$_2$O. Cl$^-$ has a smaller ionic radius than Br$^-$, thus, it is easier to accommodate to Mn^{2+} doping. The synthesis of Mn-doped CsPbBr$_3$ PMSCs is sensitive to the Mn^{2+} precursors used.

Table 1. Summary of Some Examples of Surface Passivation of Perovskite Quantum Dots, Magic Sized Clusters, and Molecular Clusters

Ligand (Molecular structure)	Impact of ligand		Ref.
	Synthesis	Transformation	
Straight chain ligands			
Oleic acid (OA); n-octanoic acid (OcA)	PQDs/PMSCs (OA/OcAm, OA/OcAm, OcA/BTYA, OA/OLA)	√	17, 51
Valeric acid (VA); Oleylamine (OLA)	PMSCs (VA/BTYA)	√	16
n-octylamine (OcAm); Butylamine (BTYA)	MCs (BTYA)	–	10
Branched termination ligands			
(3-aminopropyl)triethoxysilane (APTES); Polyhedral oligomeric silsesquioxane (POSS)	PQDs (APTES/OA, POSS/OA)	–	30
Aromatic capping ligands			
Benzylamine (BZA); Benzoic acid (BA)	PQDs (BZA/BA)	–	31
trans-cinnamic acid (TCA); 3,3-diphenylpropylamine (DPPA)	PQDs (TCA/DPPA)	–	32
Mesitylacetic acid (MAA); Phenylacetic acid (PAA)	PQDs/PMSCs (MAA/BZA, OA/BZA, PAA/BZA)	√	15
Multi-dentate ligand molecules			
12-aminododecanoic acid (12-AA)	PQDs (12-AA)	–	29
Phenylalanine (Phe); Leucine (Leu); L-lysine (Lys)	PQDs (Lys, Arg)	–	33
L-arginine (Arg)	PQDs (Phe, Leu)	–	34
Polymers — Metal-organic frameworks (MOFs); Cellulose; Poly(acrylic acid)-block-poly(styrene) (PAA-b-PS); Polystyrene-block-poly-2-vinylpyridine (PS-b-P2VP)	PQDs (MOFs)	–	45
	PQDs (PS-b-P2VP)	–	46
	PQDs (Cellulose)	–	48
	PQDs (PAA-b-PS)	–	49
Other ligands — Methylphosphonic acid (MPA); n-Hexylphosphonic acid (HPA); 1-Tetradecylphosphonic acid (TDPA); n-Octadecylphosphonic acid (ODPA)	PQDs (MPA/APTES, HPA/APTES, TDPA/APTES, ODPA/APTES)	–	40
Cationic ligands (R = Alk; R' = H or Alk)	PQDs (Cationic ligands)	–	41, 42, 43
Aluminum nitrate nonahydrate [Al(NO$_3$)$_3$·9H$_2$O, ANN]	PQDs/PMSCs (ANN/OA/OLA)	√	52

A similar preference of Mn^{2+} doping in MCs was also reported, where no characteristic Mn^{2+} d−d emission in the product was observed when MnBr$_2$ was used (Figure 9c).[67] The Mn^{2+} precursor was suggested to play a key role in the synthesis of Mn-doped MCs. Mn^{2+} doping only takes place at relatively high MnCl$_2$ concentration, and MnCl$_2$ seems to contribute to the incorporation of Mn^{2+}. When Cl$^−$ and Mn^{2+} are introduced together, Br$^−$ and Cl$^−$ are likely to undergo anion exchange in solution to form PbCl$_2$, which is beneficial to the formation of doped MCs because the bond energies of Mn−Cl and Pb−Cl are similar. The ion exchange reaction between Cl$^−$ and Br$^−$ was characterized by blue-shifted electron absorption and PL spectra of the host MCs. The Mn^{2+} doping appears to be assisted by Cl$^−$ ions in a codoping

manner. TRPL and electron paramagnetic resonance (EPR) data suggest that with excess Mn^{2+} concentrations, Mn−Mn coupling may lead to a reduction or disappearance of Mn^{2+} d−d emission, resulting in a shortened PL lifetime.

5. SUMMARY AND PERSPECTIVE

In summary, metal halide PQDs and PMSCs have demonstrated unique and intriguing optical and electronic properties. Surface passivation has proven to be a highly effective technique for their stabilization using a variety of molecular ligands with different structures and anchoring groups. The general strategy is to passivate anionic surface defects using cationic ligands and cationic surface defects using anionic ligands based on electrostatic interaction. The charge state of
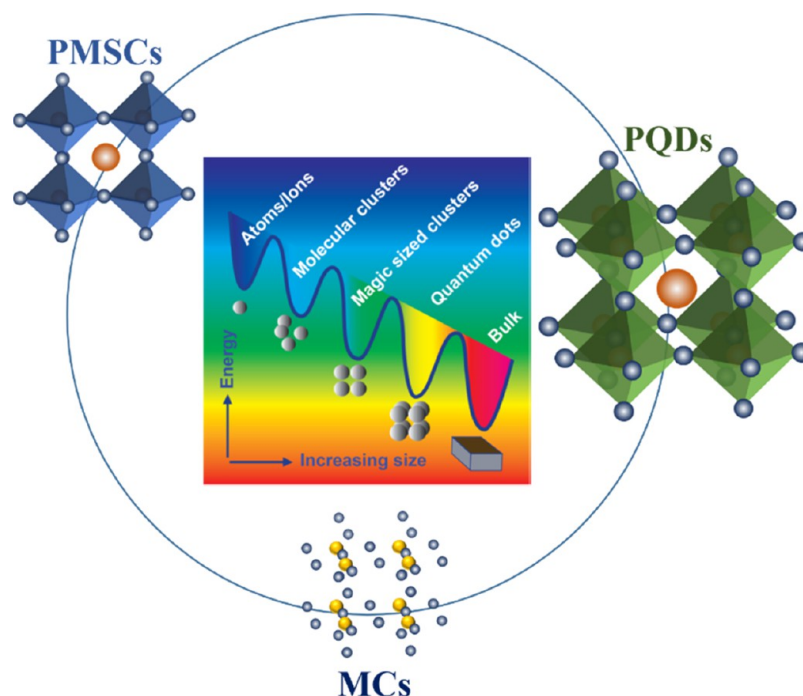
Figure 10. Schematic illustration of the relation among atoms/ions, MCs, MSCs, QDs, and bulk material. With increasing size, stability generally increases. There is likely many interesting species between atoms/ions and bulk that are yet to be uncovered.

the anchoring group of the ligands is clearly critical in determining the effectiveness of passivation. The size and shape of the ligands are also very important. The multiple defects expected on the surface of the perovskite nanocrystals require a combination of different ligands for optimal passivation ("cocktail" approach). Table 1 shows a summary of some examples of surface passivation of PQDs, PMSCs, and MCs using different ligands.

Despite extensive developments in the surface defect passivation, a comprehensive understanding of the origin of surface states of PQDs and PMSCs at the atomic scale remains to be achieved. Most capping ligands demonstrated to date are based on easily available compounds. New capping ligands with stronger and selective coordination ability are desired for optimal passivation and need to be developed in the future. Furthermore, to date, most of the work has focused on lead-based halide clusters. The strategy for surface passivation may differ for other metal-based halide clusters. The nature and energetics of trap states can also vary substantially among bromide, chloride, and iodides, which may also call for different passivation ligands and strategies.

The exact structure of PMSCs is of strong interest but is challenging to determine to date. Due to the ultrasmall size of PMSCs, PMSCs do not have a long enough ordered structure to be readily characterized by XRD or TEM. In addition, given their instability in polar solvents and at elevated temperature, PMSCs cannot be easily measured by mass spectrometry. Therefore, the exact dimension or number of Pb-octahedra in PMSCs is not yet known. To better understand the exact structure of PMSCs, further work will be required in the future both experimentally and theoretically, possibly using cryo-TEM, in situ measurement, X-ray absorption spectroscopy, or some low-temperature "trapping" or encapsulation methods in which the PMSCs are stabilized and isolated in some stable matrix like polymer or glass to allow detailed characterization.

The discovery of the lead halide MCs provided an important opportunity to study and better understand the growth mechanisms of PMSCs as well as PQDs. There is an intricate interplay among PQDs, PMSCs, and MCs. MCs can be synthesized using only PbX_2 (X for halide ions) and appropriate ligands, with no A component. With the addition of an A component precursor (e.g., MAX), MCs can be converted into PMSCs and further into PQDs. Conversely, with a higher concentration of ligands and/or stronger ligands, PQDs can be converted into PMSCs. Both PQDs and PMSCs can also be fragmented into MCs. The interconversion among MCs, PMSCs, and PQDs is strongly dependent on the experimental conditions, particularly the reactant and ligand concentrations. MCs can act as "precursors" to PMSCs while PMSCs as "precursors" to PQDs, as illustrated in Figure 1. If ligands are removed, they will all ultimately form bulk perovskites.

As illustrated in Figure 10, there is likely a large number of MCs and PMSCs between isolated or solvated atoms/ions and bulk that are yet to be uncovered, and their existence and discovery will be strongly dependent on the experimental conditions including the concentration and nature of passivating ligands. Both theoretical studies and advanced experimental techniques will be needed to better characterize MCs as well as PMSCs.

Doping provides another important method to alter and improve the properties of PQDs and clusters. To date, Mn^{2+} doping has been demonstrated successfully for PQDs, PMSCs, and MCs. There is room to better understand the doping mechanism and expand doping with other dopants or codopants to further improve their optical properties.

In general, while isolated or solvated precursor ions and bulk solid MHPs are relatively well-understood, species between them, including PQDs, PMSCs, and MCs, are much less known, especially in terms of their detailed structures. These intermediate species are interesting and potential building

blocks for more complex structures of interesting and emerging technologies ranging from quantum materials and quantum information (e.g., single photon emitters) to PVs, LEDs, detectors, lasers, and sensors. There is plenty of species between isolated ions and bulk, and their discovery is expected to lead to interesting materials for fundamental research and applications of optoelectronic devices.

■ AUTHOR INFORMATION

Corresponding Authors

Jin Z. Zhang − *Department of Chemistry and Biochemistry, University of California, Santa Cruz, California 95064, United States;* ● orcid.org/0000-0003-3437-912X; Email: zhang@ucsc.edu

Keliang Pan − *Hubei Institute of Geosciences, Wuhan 430034, P.R. China; Hubei Key Laboratory of Resource and Ecological Environment Geology, Wuhan 430034, P.R. China*; Email: pankeliang@hust.edu.cn

Authors

Li Liu − *Research Institute of Agricultural Quality Standards and Testing Technology, Hubei Academy of Agricultural Science, Wuhan 430064, P.R. China; Department of Chemistry and Biochemistry, University of California, Santa Cruz, California 95064, United States*

Ke Xu − *Multiscale Crystal Materials Research Center, Shenzhen Institute of Advanced Technology, Chinese Academy of Sciences, Shenzhen 518055, P.R. China*

Complete contact information is available at:
https://pubs.acs.org/10.1021/acsphyschemau.1c00047

Notes

The authors declare no competing financial interest.

■ ACKNOWLEDGMENTS

■ REFERENCES

(1) Khan, S. A.; Li, C.; Jalil, A.; Xin, X.; Rauf, M.; Ahmed, J.; Khan, M. A. M.; Dong, B.; Zhu, J.; Agathopoulos, S. Development of structure and tuning ability of the luminescence of lead-free halide perovskite nanocrystals (NCs). *Chemical Engineering Journal* **2021**, *420*, 127603.

(2) Zhang, H.; Nazeeruddin, M. K.; Choy, W. C. H. Perovskite Photovoltaics: The Significant Role of Ligands in Film Formation, Passivation, and Stability. *Advanced materials* **2019**, *31* (8), 1805702.

(3) Ge, C.; Fang, Q.; Lin, H.; Hu, H. Review on Blue Perovskite Light-Emitting Diodes: Recent Advances and Future Prospects. *Frontiers in Materials* **2021**, *8*, 635025.

(4) Ahmadi, M.; Wu, T.; Hu, B. A Review on Organic-Inorganic Halide Perovskite Photodetectors: Device Engineering and Fundamental Physics. *Adv. Mater.* **2017**, *29* (41), 1605242.

(5) Wang, H.; Kim, D. H. Perovskite-based photodetectors: materials and devices. *Chem. Soc. Rev.* **2017**, *46* (17), 5204−5236.

(6) Shellaiah, M.; Sun, K. W. Review on Sensing Applications of Perovskite Nanomaterials. *Chemosensors* **2020**, *8* (3), 55.

(7) Wang, X.; Bao, Z.; Chang, Y. C.; Liu, R. S. Perovskite Quantum Dots for Application in High Color Gamut Backlighting Display of Light-Emitting Diodes. *ACS Energy Letters* **2020**, *5* (11), 3374−3396.

(8) Chen, D.; Chen, X. Luminescent perovskite quantum dots: synthesis, microstructures, optical properties and applications. *Journal of Materials Chemistry C* **2019**, *7* (6), 1413−1446.

(9) Efros, A. L.; Brus, L. E. Nanocrystal Quantum Dots: From Discovery to Modern Development. *ACS Nano* **2021**, *15* (4), 6192−6210.

(10) Vickers, E. T.; Chen, Z.; Cherrette, V.; Smart, T.; Zhang, P.; Ping, Y.; Zhang, J. Z. Interplay between Perovskite Magic-Sized Clusters and Amino Lead Halide Molecular Clusters. *Research* **2021**, *2021*, 1−7.

(11) Palencia, C.; Yu, K.; Boldt, K. The Future of Colloidal Semiconductor Magic-Size Clusters. *ACS Nano* **2020**, *14* (2), 1227−1235.

(12) He, L.; Luan, C.; Rowell, N.; Zhang, M.; Chen, X.; Yu, K. Transformations Among Colloidal Semiconductor Magic-Size Clusters. *Acc. Chem. Res.* **2021**, *54* (4), 776−786.

(13) Shangguan, Z.; Zheng, X.; Zhang, J.; Lin, W.; Guo, W.; Li, C.; Wu, T.; Lin, Y.; Chen, Z. The Stability of Metal Halide Perovskite Nanocrystals-A Key Issue for the Application on Quantum-Dot-Based Micro Light-Emitting Diodes Display. *Nanomaterials* **2020**, *10* (7), 1375.

(14) Xue, J.; Wang, R.; Yang, Y. The surface of halide perovskites from nano to bulk. *Nature Reviews Materials* **2020**, *5*, 809−827.

(15) Xu, K.; Vickers, E. T.; Luo, B.; Wang, Q.; Allen, A. L. C.; Wang, H.; Cherrette, V.; Li, X.; Zhang, J. Z. Room Temperature Synthesis of Cesium Lead Bromide Perovskite Magic Sized Clusters with Controlled Ratio of Carboxylic Acid and Benzylamine Capping Ligands. *Sol. Energy Mater. Sol. Cells* **2020**, *208*, 110341−110346.

(16) Vickers, E. T.; Xu, K.; Dreskin, B. W.; Graham, T. A.; Li, X.; Zhang, J. Z. Ligand Dependent Growth and Optical Properties of Hybrid Organo-metal Halide Perovskite Magic Sized Clusters. *J. Phys. Chem. C* **2019**, *123* (30), 18746−18752.

(17) Liu, L.; Xu, K.; Vickers, E. T.; Allen, A.; Li, X.; Peng, L.; Zhang, J. Z. Varying the Concentration of Organic Acid and Amine Ligands Allows Tuning between Quantum Dots and Magic-Sized Clusters of CH3NH3PbBr3 Perovskite Implications for Photonics and Energy Conversion. *ACS Applied Nano Materials* **2020**, *3* (12), 12379−12387.

(18) Bera, S.; Pradhan, N. Perovskite Nanocrystal Heterostructures: Synthesis, Optical Properties, and Applications. *ACS Energy Letters* **2020**, *5* (9), 2858−2872.

(19) Abdrshin, A. N.; Lipatova, Z. O.; Kolobkova, E. V.; Sgibnev, E. M.; Nikonorov, N. V. The Influence of Silver Ion Exchange on the Formation and Luminescent Properties of Lead Sulfide Molecular Clusters and Quantum Dots. *Opt. Spectrosc.* **2016**, *121* (6), 826−830.

(20) Yang, X.; Zhang, M.; Shen, Q.; Li, Y.; Luan, C.; Yu, K. The precursor compound of two types of ZnSe magic-sized clusters. *Nano Research* **2022**, *15* (15), 465−474.

(21) Mahmoodi-Darian, M.; Martini, P.; Tiefenthaler, L.; Kočišek, J.; Scheier, P.; Echt, O. Solvation of Silver Ions in Noble Gases He, Ne, Ar, Kr, and Xe. *J. Phys. Chem. A* **2019**, *123* (48), 10426−10436.

(22) Yang, T.; Lu, M.; Mao, X.; Liu, W.; Wan, L.; Miao, S.; Xu, J. Synthesis of CdS Quantum Dots (QDs) via a Hot-bubbling Route and Co-sensitized Solar Cells Assembly. *Chemical Engineering Journal* **2013**, *225*, 776−783.

(23) Lipatova, Z. O.; Kolobkova, E. V.; Sidorov, A. I.; Nikonorov, N. V. The influence of sodium nanoparticles formation on luminescent properties of fluorophosphate glasses containing molecular clusters and quantum dots of lead selenide. *Opt. Spectrosc.* **2016**, *121* (2), 200−209.

(24) Protesescu, L.; Yakunin, S.; Bodnarchuk, M. I.; Krieg, F.; Caputo, R.; Hendon, C. H.; Yang, R. X.; Walsh, A.; Kovalenko, M. V. Nanocrystals of Cesium Lead Halide Perovskites (CsPbX3, X = Cl,

Br, and I): Novel Optoelectronic Materials Showing Bright Emission with Wide Color Gamut. *Nano Lett.* **2015**, *15* (6), 3692−3696.

(25) Zhang, F.; Zhong, H. Z.; Chen, C.; Wu, X. G.; Hu, X. M.; Huang, H. L.; Han, J. B.; Zou, B. Z.; Dong, Y. P. Brightly Luminescent and Color Tunable Colloidal CH3NH3PbX3 (X = Br, I, Cl) Quantum Dots: Potential Alternatives for Display Technology. *ACS Nano* **2015**, *9* (4), 4533−4542.

(26) Bodunov, E. N.; Simões Gamboa, A. L. Kinetics of Photoluminescence Decay of Colloidal Quantum Dots: Reversible Trapping of Photogenerated Charge Carriers. *Semiconductors* **2019**, *53* (16), 2133−2136.

(27) Bodunov, E. N.; Simões Gamboa, A. L. Photoluminescence Decay of Colloidal Quantum Dots: Reversible Trapping and the Nature of the Relevant Trap States. *J. Phys. Chem. C* **2019**, *123* (41), 25515−25523.

(28) Zhang, J. Z. A "Cocktail" Approach to Effective Surface Passivation of Multiple Surface Defects of Metal Halide Perovskites Using a Combination of Ligands. *J. Phys. Chem. Lett.* **2019**, *10*, 5055−5063.

(29) Luo, B.; Naghadeh, S. B.; Allen, A. L.; Li, X.; Zhang, J. Z. Peptide-Passivated Lead Halide Perovskite Nanocrystals Based on Synergistic Effect between Amino and Carboxylic Functional Groups. *Adv. Funct. Mater.* **2017**, *27* (6), 1604018.

(30) Luo, B.; Pu, Y. C.; Lindley, S. A.; Yang, Y.; Lu, L.; Li, Y.; Li, X.; Zhang, J. Z. Organolead Halide Perovskite Nanocrystals: Branched Capping Ligands Control Crystal Size and Stability. *Angew. Chem., Int. Ed.* **2016**, *55* (31), 8864−8868.

(31) Vickers, E. T.; Graham, T. A.; Chowdhury, A. H.; Bahrami, B.; Dreskin, B. W.; Lindley, S.; Naghadeh, S. B.; Qiao, Q.; Zhang, J. Z. Improving Charge Carrier Delocalization in Perovskite Quantum Dots by Surface Passivation with Conductive Aromatic Ligands. *ACS Energy Letters* **2018**, *3* (12), 2931−2939.

(32) Vickers, E. T.; Enlow, E. E.; Delmas, W. G.; DiBenedetto, A. C.; Chowdhury, A. H.; Bahrami, B.; Dreskin, B. W.; Graham, T. A.; Hernandez, I. N.; Carter, S. A.; Ghosh, S.; Qiao, Q.; Zhang, J. Z. Enhancing Charge Carrier Delocalization in Perovskite Quantum Dot Solids with Energetically Aligned Conjugated Capping Ligands. *ACS Energy Letters* **2020**, *5* (3), 817−825.

(33) Jancik Prochazkova, A.; Demchyshyn, S.; Yumusak, C.; MáSilko, J.; Brüggemann, O.; Weiter, M.; Kaltenbrunner, M.; Sariciftci, N. S.; Krajcovic, J.; Salinas, Y.; Kovalenko, A. Proteinogenic Amino Acid Assisted Preparation of Highly Luminescent Hybrid Perovskite Nanoparticles. *ACS Applied Nano Materials* **2019**, *2* (7), 4267−4274.

(34) Sharma, A. K.; Bansal, P.; Nim, G. K.; Kar, P. Essential Amino Acid-Enabled Lead Bromide Perovskite Nanocrystals with High Stability. *Particle & Particle Systems Characterization* **2019**, *36* (12), 1900328.

(35) Shih, Y. C.; Lan, Y. B.; Li, C. S.; Hsieh, H. C.; Wang, L.; Wu, C. I.; Lin, K. F. Amino-Acid-Induced Preferential Orientation of Perovskite Crystals for Enhancing Interfacial Charge Transfer and Photovoltaic Performance. *Small* **2017**, *13* (22), 1604305.

(36) Wang, S.; Zhou, L.; Huang, F.; Xin, Y.; Jin, P.; Ma, Q.; Pang, Q.; Chen, Y.; Zhang, J. Z. Hybrid organic-inorganic lead bromide perovskite supercrystals self-assembled with L-cysteine and their good luminescence properties. *Journal of Materials Chemistry C* **2018**, *6*, 10994−11001.

(37) Liu, L.; Xu, K.; Allen, A. L.; Li, X.; Xia, H.; Peng, L.; Zhang, J. Z. Enhancing the Photoluminescence and Stability of Methylammonium Lead Halide Perovskite Nanocrystals with Phenylalanine. *J. Phys. Chem. C* **2021**, *125* (4), 2793−2801.

(38) Manoli, A.; Papagiorgis, P.; Sergides, M.; Bernasconi, C.; Athanasiou, M.; Pozov, S.; Choulis, S. A.; Bodnarchuk, M. I.; Kovalenko, M. V.; Othonos, A.; Itskos, G. Surface Functionalization of CsPbBr3 Nanocrystals for Photonic Applications. *ACS Applied Nano Materials* **2021**, *4* (5), 5084−5097.

(39) Krieg, F.; Sercel, P. C.; Burian, M.; Andrusiv, H.; Bodnarchuk, M. I.; Stoferle, T.; Mahrt, R. F.; Naumenko, D.; Amenitsch, H.; Raino, G.; Kovalenko, M. V. Monodisperse Long-Chain Sulfobetaine-Capped CsPbBr3 Nanocrystals and Their Superfluorescent Assemblies. *ACS Central Science* **2021**, *7* (1), 135−144.

(40) Xu, K.; Vickers, E. T.; Rao, L.; Lindley, S. A.; Allen, A. C.; Luo, B.; Li, X.; Zhang, J. Z. Synergistic Surface Passivation of CH3NH3PbBr3 Perovskite Quantum Dots with Phosphonic Acid and (3-Aminopropyl)triethoxysilane. *Chem.—Eur. J.* **2019**, *25* (19), 5014−5021.

(41) Toso, S.; Baranov, D.; Manna, L. Metamorphoses of Cesium Lead Halide Nanocrystals. *Acc. Chem. Res.* **2021**, *54* (3), 498−508.

(42) Stelmakh, A.; Aebli, M.; Baumketner, A.; Kovalenko, M. V. On the Mechanism of Alkylammonium Ligands Binding to the Surface of CsPbBr3 Nanocrystals. *Chem. Mater.* **2021**, *33* (15), 5962−5973.

(43) Pradhan, N. Alkylammonium Halides for Facet Reconstruction and Shape Modulation in Lead Halide Perovskite Nanocrystals. *Acc. Chem. Res.* **2021**, *54* (5), 1200−1208.

(44) Manna, L.; Cheon, J.; Schaak, R. E. Why Do We Care about Studying Transformations in Inorganic Nanocrystals? *Acc. Chem. Res.* **2021**, *54* (7), 1543−1544.

(45) Rambabu, D.; Bhattacharyya, S.; Singh, T.; M. L., C.; Maji, T. K. Stabilization of MAPbBr3 Perovskite Quantum Dots on Perovskite MOFs by a One-Step Mechanochemical Synthesis. *Inorg. Chem.* **2020**, *59* (2), 1436−1443.

(46) Hou, S.; Guo, Y.; Tang, Y.; Quan, Q. Synthesis and Stabilization of Colloidal Perovskite Nanocrystals by Multidentate Polymer Micelles. *ACS Appl. Mater. Interfaces* **2017**, *9* (22), 18417−18422.

(47) Huang, S.; Tan, L.; Zhang, L.; Wu, J.; Zhang, L.; Tang, Y.; Wang, H.; Liang, Y. Molecularly imprinted mesoporous silica embedded with perovskite CsPbBr3 quantum dots for the fluorescence sensing of 2,2-dichlorovinyl dimethyl phosphate. *Sens. Actuators, B* **2020**, *325*, 128751.

(48) Park, B.; Kang, S.-M.; Lee, G. W.; Kwak, C. H.; Rethinasabapathy, M.; Huh, Y. S. Fabrication of CsPbBr3 Perovskite Quantum Dots/Cellulose-Based Colorimetric Sensor: Dual-Responsive On-Site Detection of Chloride and Iodide Ions. *Ind. Eng. Chem. Res.* **2020**, *59* (2), 793−801.

(49) Imran, M.; Mai, B. T.; Goldoni, L.; Cirignano, M.; Jalali, H. B.; Di Stasio, F.; Pellegrino, T.; Manna, L. Switchable Anion Exchange in Polymer-Encapsulated APbX3 Nanocrystals Delivers Stable All-Perovskite White Emitters. *ACS Energy Letters* **2021**, *6* (8), 2844−2853.

(50) Peng, L.; Geng, J.; Ai, L.; Zhang, Y.; Xie, R.; Yang, W. Room temperature synthesis of ultra-small, near-unity single-sized lead halide perovskite quantum dots with wide color emission tunability, high color purity and high brightness. *Nanotechnology* **2016**, *27* (33), 335604.

(51) Xu, Y.; Zhang, Q.; Lv, L.; Han, W.; Wu, G.; Yang, D.; Dong, A. Synthesis of ultrasmall CsPbBr3 nanoclusters and their transformation to highly deep-blue-emitting nanoribbons at room temperature. *Nanoscale* **2017**, *9* (44), 17248−17253.

(52) Xu, K.; Allen, A. C.; Luo, B.; Vickers, E. T.; Wang, Q.; Hollingsworth, W. R.; Ayzner, A. L.; Li, X.; Zhang, J. Z. Tuning from Quantum Dots to Magic Sized Clusters of CsPbBr3 Using Novel Planar Ligands Based on the Trivalent Nitrate Coordination Complex. *J. Phys. Chem. Lett.* **2019**, *10* (15), 4409−4416.

(53) Nguyen, T. P.; Ozturk, A.; Park, J.; Sohn, W.; Lee, T. H.; Jang, H. W.; Kim, S. Y. Facile synthesis of CsPbBr3/PbSe composite clusters. *Sci. Technol. Adv. Mater.* **2018**, *19* (1), 10−17.

(54) Peng, L.; Dutta, A.; Xie, R.; Yang, W.; Pradhan, N. Dot-Wire-Platelet-Cube: Step Growth and Structural Transformations in CsPbBr3 Perovskite Nanocrystals. *ACS Energy Letters* **2018**, *3* (8), 2014−2020.

(55) Tong, Y.; Ehrat, F.; Vanderlinden, W.; Cardenas-Daw, C.; Stolarczyk, J. K.; Polavarapu, L.; Urban, A. S. Dilution-Induced Formation of Hybrid Perovskite Nanoplatelets. *ACS Nano* **2016**, *10* (12), 10936−10944.

(56) Ma, X.; Yang, L.; Lei, K.; Zheng, S.; Chen, C.; Song, H. Doping in inorganic perovskite for photovoltaic application. *Nano Energy* **2020**, *78*, 105354.

(57) Xu, L.; Yuan, S.; Zeng, H.; Song, J. A comprehensive review of doping in perovskite nanocrystals/quantum dots: evolution of structure, electronics, optics, and light-emitting diodes. *Materials Today Nano* **2019**, *6*, 100036.

(58) Xie, Y.; Peng, B.; Bravic, I.; Yu, Y.; Dong, Y.; Liang, R.; Ou, Q.; Monserrat, B.; Zhang, S. Highly Efficient Blue-Emitting CsPbBr3 Perovskite Nanocrystals through Neodymium Doping. *Advanced science* **2020**, *7* (20), 2001698.

(59) Bi, C.; Wang, S.; Li, Q.; Kershaw, S. V.; Tian, J.; Rogach, A. L. Thermally Stable Copper(II)-Doped Cesium Lead Halide Perovskite Quantum Dots with Strong Blue Emission. *J. Phys. Chem. Lett.* **2019**, *10* (5), 943−952.

(60) Deng, J.; Xun, J.; Shen, W.; Li, M.; He, R. Sb3+-Doped dual-phase perovskite nanocrystals with strong green luminescence and excellent Water and thermal stability. *Mater. Res. Bull.* **2021**, *140*, 111296.

(61) Wang, X.; Xu, Z.; Zhuo, S.; Hu, P.; Yang, Y.; Zhou, B.; Zhang, W.-H. Strain Modulation for High Brightness Blue Luminescence of Pr3+-Doped Perovskite Nanocrystals via Siloxane Passivation. *ACS Applied Electronic Materials* **2021**, *3* (9), 3815−3823.

(62) Mir, W. J.; Sheikh, T.; Arfin, H.; Xia, Z.; Nag, A. Lanthanide doping in metal halide perovskite nanocrystals: spectral shifting, quantum cutting and optoelectronic applications. *NPG Asia Materials* **2020**, *12* (1), 9.

(63) Ding, H. W.; Liu, W. W.; Zheng, Y. K.; Li, C. M.; Jiang, H.; Wang, X. M. Transition metal halides doped highly stable all-inorganic perovskite nanocrystals for fabrication of white light-emitting diodes. *Journal of Materials Chemistry C* **2019**, *7* (6), 1690.

(64) Montanarella, F.; McCall, K. M.; Sakhatskyi, K.; Yakunin, S.; Trtik, P.; Bernasconi, C.; Cherniukh, I.; Mannes, D.; Bodnarchuk, M. I.; Strobl, M.; Walfort, B.; Kovalenko, M. V. Highly Concentrated, Zwitterionic Ligand-Capped Mn2+:CsPb(BrxCl1-x)3 Nanocrystals as Bright Scintillators for Fast Neutron Imaging. *ACS Energy Letters* **2021**, *6* (12), 4365−4373.

(65) Pradhan, N. Mn-Doped Semiconductor Nanocrystals: 25 Years and Beyond. *J. Phys. Chem. Lett.* **2019**, *10* (10), 2574−2577.

(66) Xu, K.; Vickers, E. T.; Luo, B.; Allen, A. C.; Chen, E.; Roseman, G.; Wang, Q.; Kliger, D. S.; Millhauser, G. L.; Yang, W.; Li, X.; Zhang, J. Z. First Synthesis of Mn-Doped Cesium Lead Bromide Perovskite Magic Sized Clusters at Room Temperature. *J. Phys. Chem. Lett.* **2020**, *11* (3), 1162−1169.

(67) Liu, L.; Pan, K.; Xu, K.; Peng, X.; Zhang, J. Z. Synthesis and Optical Properties of Mn2+-Doped Amino Lead Halide Molecular Clusters Assisted by Chloride Ion. *J. Phys. Chem. Lett.* **2021**, *12*, 7497−7503.